Hindawi Publishing Corporation
Journal of Nanomaterials
Volume 2014, Article ID 903208, 11 pages
http://dx.doi.org/10.1155/2014/903208

Research Article

Upconversion luminescence and Visible-Infrared Properties of β-$NaLuF_4$:Er^{3+} Microcrystals Synthesized by the Surfactant-Assisted Hydrothermal Method

Han Lin,[1] Xiaohong Yan,[1,2] Jin Zheng,[2] Changjie Dai,[1] and Yuan Chen[1]

[1] *College of Science, Nanjing University of Aeronautics and Astronautics, Nanjing 211106, China*
[2] *School of Electronic Science and Engineering, Nanjing University of Posts and Telecommunications, Nanjing 210046, China*

Correspondence should be addressed to Xiaohong Yan; xhyan@nuaa.edu.cn

Received 21 February 2014; Revised 20 May 2014; Accepted 22 May 2014; Published 18 June 2014

Academic Editor: Alireza Talebitaher

We report the obtention of β-$NaLuF_4$ microcrystals doped with Er^{3+} ions by the surfactant-assisted hydrothermal method. It was found that shape modulation could be realized by changing the surfactants (ethylenediaminetetraacetic acid, polyvinylpyrrolidone, and trisodium citrate) introduced into the reaction system. The surfactants can strongly control the size and shape of as-prepared samples through absorbing on the surface of primary particles and/or coordinating with rare earth ions. Hexagonal prism-like β-$NaLuF_4$:Er^{3+} microcrystals demonstrate intense upconverted luminescence (UCL) pumped by 1.54 μm infrared laser in comparison with hexagonal tube-like, disk-like, and sphere-like microcrystals, which exhibit great distinction. More interestingly, a synergistic effect combined dual mode (i.e., downconversion and upconversion) with 8% absolute enhancement rate of the red emission centered at 659 nm ($^4F_{9/2} \rightarrow {}^4I_{15/2}$) is witnessed in hexagonal prisms β-$NaLuF_4$:Er^{3+} phosphors by employing the dual wavelength 416 nm and 1.54 μm excitation source for the first time.

1. Introduction

Rare earth fluorides including REF_3 and $AREF_4$ (A = alkali; RE = rare earth) have been regarded as excellent downconversion (DC) and upconversion (UC) luminescent hosts for various optically active Ln^{3+} ions [1–6]. They normally possess low phonon energy, low probability of nonradiative decay, and high chemical stabilities, and the luminescent quantum yields higher than that in oxide hosts and most inorganic matrices. Thus, rare earth fluorides have attracted much attention of scientific community due to their potential applications in the fields of solid-state lasers, multicolor three dimensional displays, optical storage, and biological fields including fluorescent labels, therapy, and drug delivery [7–10]. One example for this class of fluoride compounds is $NaLuF_4$, which is an ideal UC host material [11–16]. Shi et al. [11] synthesized hexagonal nanoplates β-$NaLuF_4$:Yb^{3+}/Tm^{3+} crystals by hydrothermal method using oleic acid as the surfactant and demonstrated that β-$NaLuF_4$ nanocrystals might be a better kind of upconversion material than their β-$NaYF_4$ counterpart. Li et al. [15] prepared multiform morphologies β-$NaLuF_4$ by changing the solution pH values, F^- sources, and organic additives and studied the morphological evolvement and the growth mechanism for the synthesized lutetium fluorides under different conditions in detail.

In this work, we present our recent efforts on the fabrication of $NaLuF_4$ crystals with controllable sizes and enhanced PL properties. Emission intensity and energy efficiency are used as measures of the phosphors performance. They are important performance characteristics that determine which applications are appropriate. In most cases, the thermalization losses and subbandgap light transmission are the major bottleneck effect on energy efficiency [17–20]. Erbium (Er) possesses several long-lived intermediate levels and metastable high-energy levels, and the energy gap between the ground level $^4I_{15/2}$ and the first excited level $^4I_{13/2}$ is matched well with the absorption of 1.54 μm photon, so it can be considered as a promising candidate among REs

Table 1: Summary of morphologies and their corresponding detailed experimental conditions of samples[a].

Sample	Agents	Agents/Recl$_3$ molar ratio	Phase	Morphology	Mean size (μm)	Graph
S1	EDTA	1 : 1	Hexagonal	Hexagonal prisms	L: 9	Figure 2(a)
S2	EDTA	2 : 1	Hexagonal	Hexagonal prisms	L: 3.5	Figure 2(b)
S3	EDTA	3 : 1	Hexagonal	Hexagonal prisms	L: 1	Figure 2(c)
S4	PVP	1 : 1	Hexagonal	Tubes with cracks	H: 10	Figure 2(d)
S5	PVP	2 : 1	Hexagonal	Tubes with cracks	H: 5	Figure 2(e)
S6	PVP	3 : 1	Hexagonal	Irregular hexagonal tubes	H: 1.5	Figure 2(f)
S7	Ct^{3-}	1 : 1	Orthorhombic (LuF_3)	Spheres	D: 3.5	Figure 2(g)
S8	Ct^{3-}	2 : 1	Hexagonal	Spheres with coarse surface	D: 2	Figure 2(h)
S9	Ct^{3-}	3 : 1	Hexagonal	Perfect disks	D: 1.5	Figure 2(i)

D: diameter; H: height; L: side length.
[a]All samples were hydrothermally treated at 190°C for 24 h.

for UC of photons [21–25]. The current researches mainly focus on the single mode UC or DC. No matter which mode both can enhance and improve the spectral response characteristics of materials. If we combine the two kinds of conversion mechanisms, UC and DC can be achieved in specific materials at the same time. This will make the high-energy and low-energy photons convert to middle-energy photons ultimately, and the middle-energy photon is needed for photovoltaic materials. Therefore, our group proposed a new mechanism named photon-excited synergistic effect [20].

In this paper, we report on the effect of different surfactants, such as ethylenediaminetetraacetic acid (EDTA), polyvinylpyrrolidone (PVP-K30), and trisodium citrate (hereinafter shortened form Cit^{3-}), on the growth process and PL properties at room temperature of β-$NaLuF_4$ microcrystals synthesized by the hydrothermal method. The as-prepared hexagonal prisms β-$NaLuF_4$ crystals have highly efficient UC luminescence and synergistic effect by employing the 416 nm and 1.54 μm coexcitation source.

2. Experimental Details

2.1. Synthesis of β-$NaLuF_4$ Microcrystals Doped with Er^{3+} Ions. Rare earth oxides Lu_2O_3 (99.99%) and Er_2O_3 (99.99%) were purchased from Beijing Lansu Co., China. Rare earth chlorides ($LnCl_3$, Ln:Lu/Er) were prepared by dissolving the corresponding metal oxide in 10% HCl solution at elevated temperature and then evaporating the water completely. NaF (98% purity), NaOH (96% purity), EDTA (99% purity), PVP (95% purity), and Cit^{3-} (99% purity) were purchased from Sinopharm Chemical Reagent Co., China. All chemicals were of analytical grade and were used without further purification. Deionized water (H_2O) was used throughout.

In the typical experiment of $NaLuF_4$:Er^{3+} micromaterials, a predetermined amount of EDTA was first dissolved in 18 mL distilled water under magnetic stirring to form a solution of desired molar concentration and then stoichiometric amounts of $LuCl_3$ and $ErCl_3$ were added to the solution. Under vigorous stirring for 30 min, 10 mL aqueous solution containing NaF was added dropwise into the above mixture. Then, the pH value of the suspension was adjusted to 7 through the addition of 2 M NaOH solution. The precursor solution was stirred magnetically for 10 min and then transferred to a Teflon lined stainless steel autoclave for hydrothermal treatment maintained at 190°C for 24 h. After the hydrothermal treatment, the autoclave was cooled naturally to room temperature. A light pink colored precipitate settled at the bottom, which was collected and washed repeatedly with distilled water and ethanol to remove the impurities and excessive surfactant. The sample was finally dried at 50°C for 12 h for further characterization. When PVP and Cit^{3-} were selected as chelators, the synthesis procedure was basically identical to the above description. Table 1 shows the parameters of hydrothermal synthesis and characteristics of the powders. And the samples prepared under the specific reaction conditions were denoted as S1–S9, respectively.

2.2. Characterizations. X-ray powder diffraction (XRD) measurements were performed on an Ultima-III (Rigaku) diffractometer at a scanning rate of 10° min^{-1} in the 2θ range from 10° to 70°, with graphite monochromatic Cu Kα radiation (λ = 0.15405 nm). The morphologies were obtained using scanning electron microscopy (SEM, S-3400N II, Hitachi, Japan). Transmission electron microscopy (TEM) and high-resolution transmission electron microscopy (HRTEM) were recorded on a JEOL JEM-200CX with a field emission gun operating at 200 kV. For the UC emission measurement, all the samples were pressed into pellets with 1 cm diameter and 5 mm thickness. The excitation spectra and emission spectra of samples are measured by an Omni-λ3007 spectrophotometer with a CW Xe lamp and infrared lasers with the wavelength at 1.54 μm employed as the excitation source. The dependence of upconverted emission intensity on pumping powers for different samples was obtained by changing the excitation powers. All the measurements above were performed at room temperature.

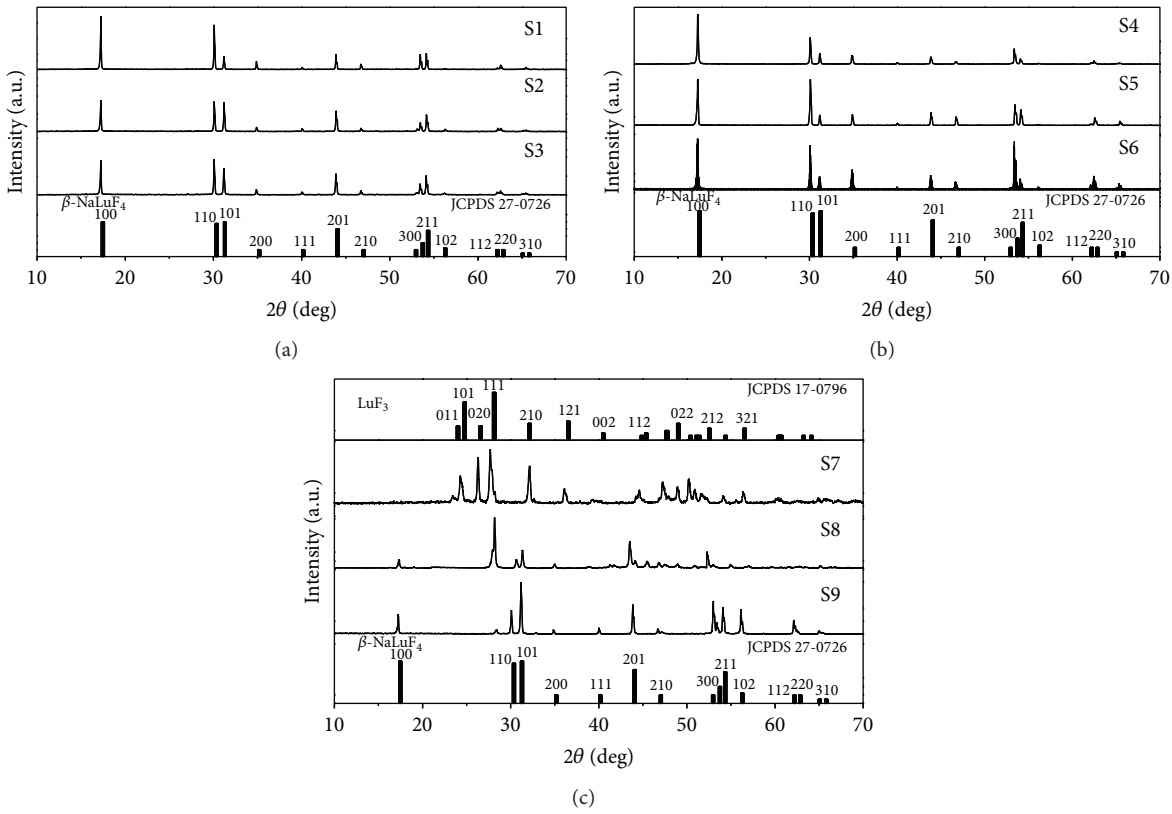

Figure 1: XRD patterns of the as-synthesized products obtained in the presence of different surfactants (EDTA: S1 to S3, PVP: S4 to S6, and Ct^{3-}: S7 to S9). The standard pattern of hexagonal $NaLuF_4$ (JCPDS card 27-0726) and orthorhombic LuF_3 (JCPDS card 17-0796) is also presented for comparison.

3. Results and Discussions

3.1. XRD Patterns Analyses. Figure 1 exhibits XRD patterns of all the prepared products corresponding to Table 1. The regularity indicated from the results is described as follows. For the samples prepared in the presence of EDTA (Figure 1(a)) and PVP (Figure 1(b)) with different agents/Ln^{3+} molar ratio, the strong and sharp diffraction peaks suggest that the pure hexagonal structure of $NaLuF_4$ (JCPDS 27-0726) is successfully achieved through the proposed direct hydrothermal process and the crystal planes for each peak are marked. Besides, the enhanced intensity of peak at $(\bar{1}00)$ and $(\bar{1}10)$ can be observed in comparison with the standard value, in which the diffraction peaks $(\bar{1}00)$ and $(\bar{1}01)$ are particularly strong. This result implies that the samples tend to be preferentially oriented. As shown in Figure 1(c), unexpectedly, the as-synthesized samples prepared in the presence of Cit^{3-} consist of two different phases, that is, the orthorhombic structure (space group *Pnma*) of LuF_3 (S7) and the hexagonal structure of $NaLuF_4$ (S8 and S9), which are in good agreement with the standard literature data. This result demonstrates that Cit^{3-} plays an important role in the phase for the formation of β-$NaLuF_4$, and it may provide a Na^+ source. When the concentration of Cit^{3-} is relatively low, there is no sufficient Na^+ source to form $NaLuF_4$, but LuF_3. The calculated cell lattice constants of the samples are summarized in Table 2, and the standard data for hexagonal structure of β-$NaLuF_4$ and orthorhombic structure of LuF_3 are also given for comparison. Obviously, the calculated cell lattice constants of the samples are consistent with the standard data.

Table 2: Unit cell lattice constants and crystallite sizes for hexagonal phase of $NaLuF_4$ and orthorhombic phase of LuF_3 prepared using different surfactants, respectively.

Samples	a (Å)	c (Å)	Cell volume (Å^3)
JCPDS 27-0726	5.9010	3.4530	104.13
S1	5.9291	3.4597	105.33
S2	5.9278	3.4583	105.24
S3	5.9354	3.4595	105.54
S4	5.9341	3.4509	105.23
S5	5.9341	3.4545	105.06
S6	5.9341	3.4509	105.23
S8	5.9661	3.4191	105.39
S9	5.9284	3.4597	105.30
JCPDS 17-0796	6.1810	4.4460	184.97
S7	6.1019	4.5715	188.75

The SEM images of microcrystals prepared using different surfactants are given in Figure 2. It can be seen that all samples exhibit relatively uniform, well-dispersed morphology

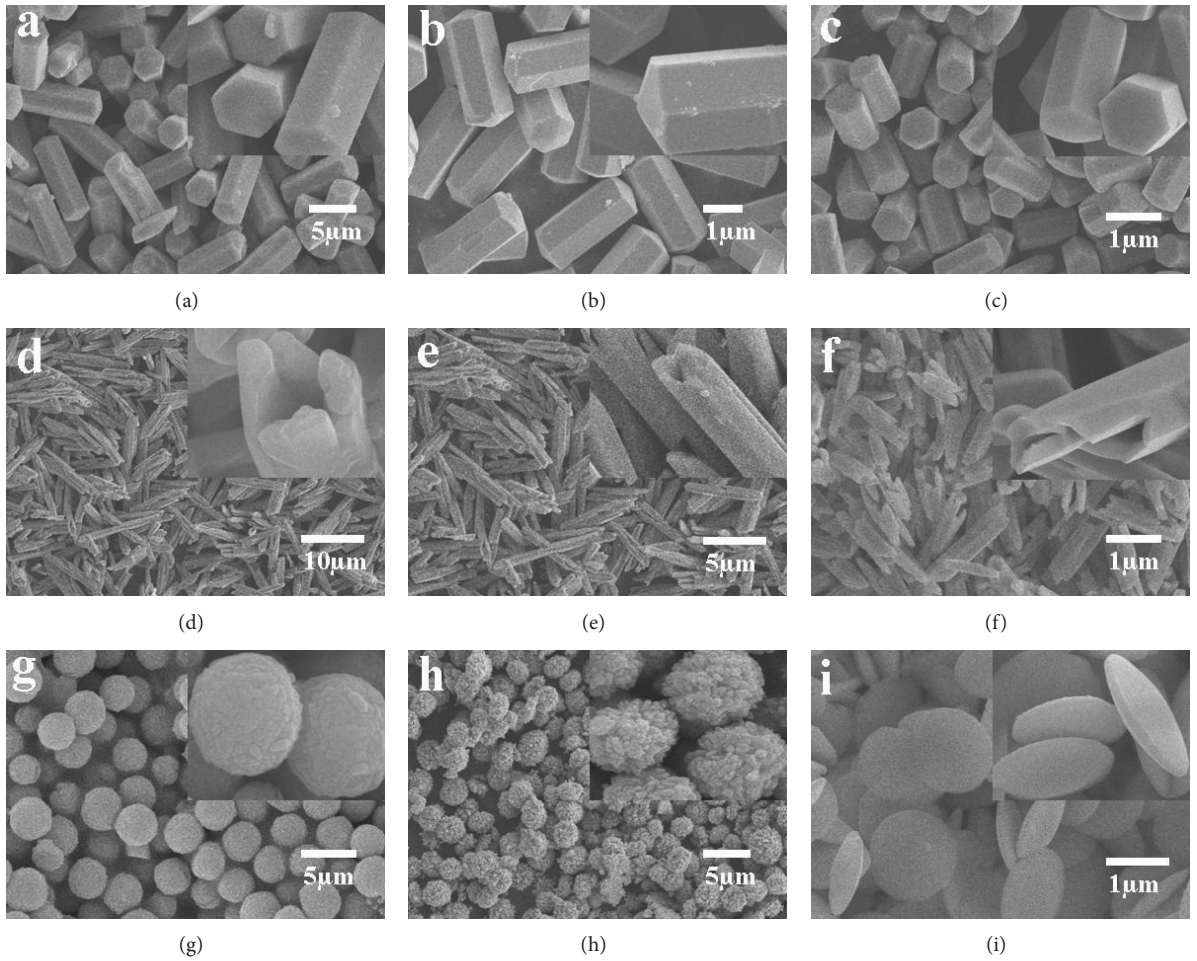

Figure 2: SEM images of as-prepared microcrystals using different surfactants with different agents/Ln^{3+} molar ratio: (a) S1, (b) S2, (c) S3, (d) S4, (e) S5, (f) S6, (g) S7, (h) S8, and (i) S9. Insets are corresponding high magnification SEM images of the microstructures.

within micrometer size range, yet the specific shapes and sizes of the samples are much different. This distinction is derived from the surfactant, since it is the only difference during the synthesis process. For the samples prepared with EDTA (sample S1–S3), uniform hexagonal prisms are obtained with 9 μm, 3.5 μm, and 1 μm in length, respectively, except that both ends of S2 are sharp. Samples prepared with PVP (S4–S6) consist of similar tube-shaped aggregates. The diameters of the three tubes are much closer (~0.5 μm), while the lengths differ greatly. As for the samples prepared with Ct^{3-} (S7–S9), they are different. Sphere-like β-$NaLuF_4$: Er^{3+} microcrystals are obtained in S7-S8, while S9 consists of fairly uniform and smooth microdisks. The peripheral surface of S8 is rough due to the composition of many small nanoparticles. This finding indicated that any change may result in different morphology and uniformity even when keeping other parameters the same. The morphological difference is caused by the physical and chemical properties of different ligands, and the effects of different surfactants will be discussed thoroughly in the following section.

TEM images, HRTEM images, and SAED patterns of the $NaLuF_4$:Er^{3+} microcrystals (S3, S6, S8, and S9) are demonstrated in Figure 3, which provide an insight of different structures. TEM image of sample S3 (Figure 3(a)) confirm it as a prism-like structure, which is in good agreement with SEM image. The ED patterns insets in Figure 3(a) show clear and regular diffraction spots, reveal the single crystalline nature of the microprism, and can be indexed as the pure hexagonal structure. The HRTEM image of a single particle confirms the distance of 0.50 nm between the adjacent lattice planes, ascribed to that of (110) crystal planes. Unlike sample S3, the tube-like structure of sample S6 is irregular (Figure 3(b)), and ED pattern exhibits the single crystalline nature of the microtube. HRTEM image recorded from the tip of an individual tube verified the lattice fringe separation of 0.52 nm. This plane coincides well with the distances between (100) crystal planes. Figures 3(c) and 3(d) exhibit the TEM images of samples prepared with Ct^{3-} (samples S8 and S9). We can see that both TEM images show the obvious spherical shape with a uniform size distribution.

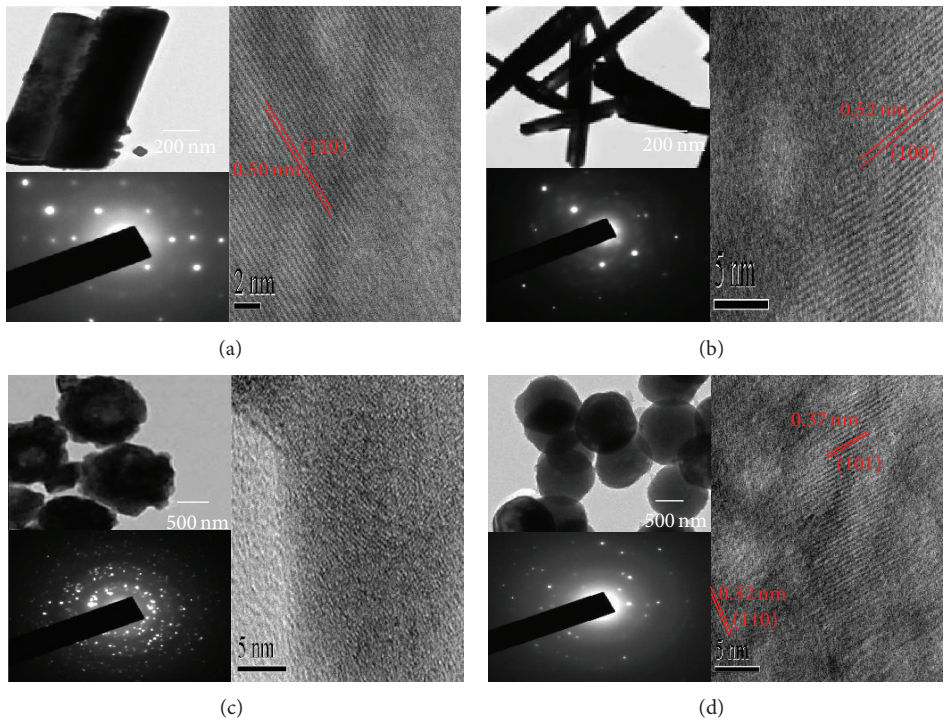

Figure 3: The TEM images, HRTEM images, and ED patterns of as-prepared β-$NaLuF_4$ microcrystals using different surfactants: (a) S3, (b) S6, (c) S8, and (d) S9.

It should be noted that the ED patterns are the polycrystalline. The lattice fringes of the sphere-like sample cannot be seen clearly due to the desultory accumulation of particles. The interplanar distance of the disk-like sample is 0.37 nm and 0.32 nm, which corresponds to the d-spacing value of the (101) and (201) planes, respectively.

3.2. Growth Mechanism of β-$NaLuF_4$ Microcrystals. Based on the above analysis, a possible growth mechanism for the microcrystals was proposed to explain the effect of different surfactants on the shape and size in detail (Figure 4). Firstly Figure 4(a) shows the coordination structures of EDTA, PVP, and Ct^{3-}. EDTA molecule possesses four carboxyl groups (–COOH) and two lone pairs of electrons on two nitrogen atoms which can act as binding sites and help to form hydrogen bonds [26]. PVP-K30 is a type of nonionic surfactant with long carbon chains and strong selective adsorption, and lanthanide ions were coordinated with the pyrrolidone groups of PVP [27]. A Ct^{3-} molecule has four binding sites, including one hydroxyl group and three COO^-, among which three sites can be bound with lanthanide ions. After formation of the nuclei (Figure 4(b)), the hydrothermal conditions performed at 190°C for 24 h inside the stainless autoclave intensify the effective collision frequency involving the anisotropic nanoparticles in suspension, producing a mutual aggregation between them. The self-assembly process can occur in a spontaneous way under hydrothermal conditions, where several nanocrystals are aggregated in a same or different crystallographic plane which can drive the growth of oriented aggregate [28]. The Ln^{3+}-EDTA complex can significantly decrease the concentration of free RE^{3+} ions and reduce the crystal growth rate, leading to the effective separation of nucleation and growth steps and thus facilitating the synthesis process of crystals. PVP-K30 can be adsorbed onto the surface of nuclei particles to further control its morphology. Furthermore, PVP-K30 can facilitate the nucleation and growth of rare earth compounds on each surface to form tube-like crystals. The Ct^{3-} molecule can also control both the crystal nucleation and the growth in the reaction system and it can cap on the side of precursor particles and lead to the selective growth rate of various crystallographic facets.

3.3. UC Luminescence Properties. The upconversion (UC) luminescence spectra for the samples (S3, S6, S8, and S9) were recorded upon 1.54 μm pumping with power density of 16 mW/mm^2. Obviously, the four samples exhibit quite different emission intensities and peak positions. Figure 5 shows the upconversion emission spectra of β-$NaLuF_4$:x mol%Er^{3+} (x = 6, 12, 24, 36) microcrystals. As can be observed, in hexagonal prisms (S3; Figure 5(a)) and hexagonal tubes (S6; Figure 5(b)), there were three well-known intense emission bands centered at 541 nm, 659 nm, and 805 nm, which are

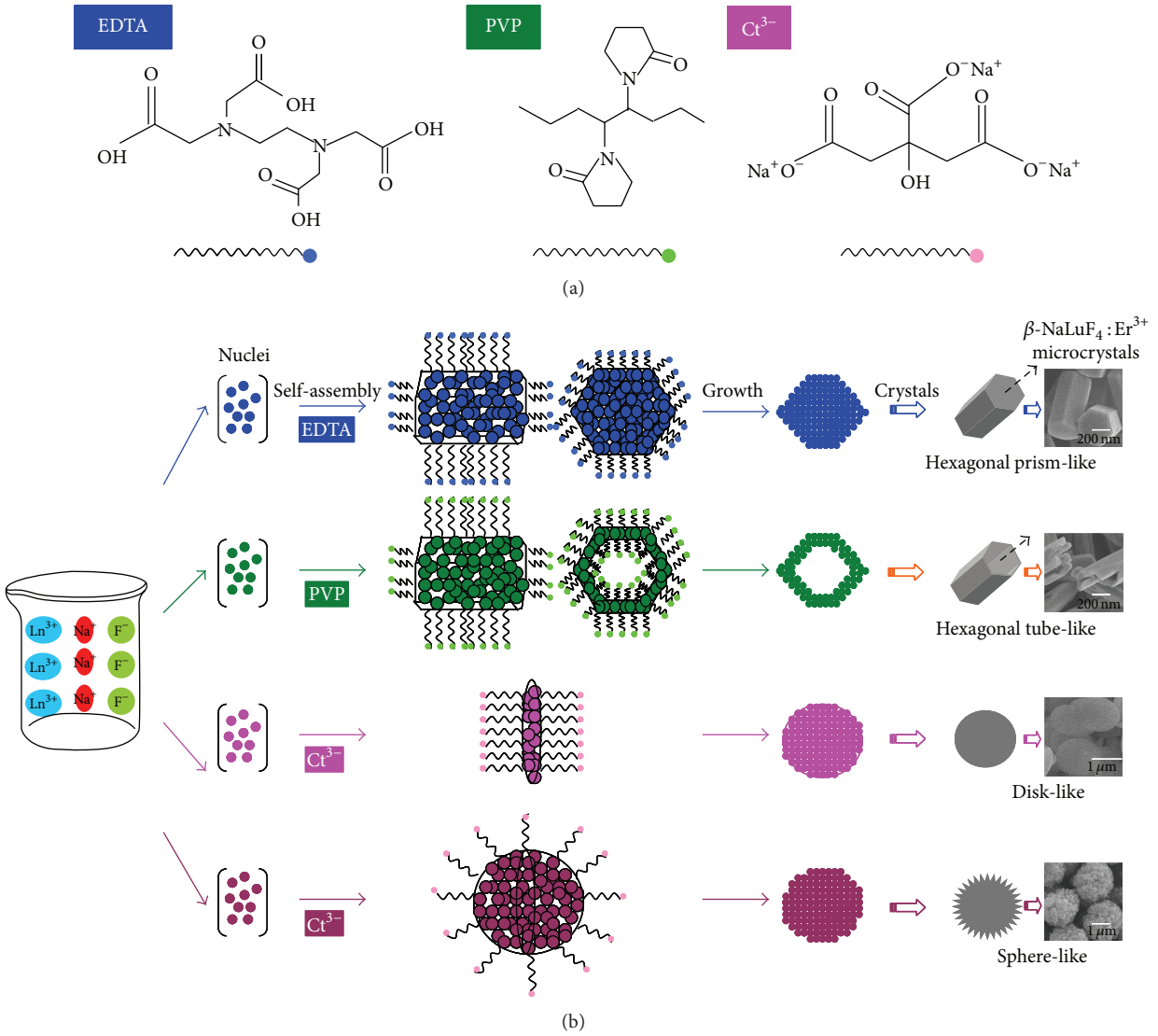

FIGURE 4: (a) Newman representations for coordination compound structure of EDTA, PVP, and Ct^{3-}. (b) Schematic illustration of the main stages involved in the growth mechanism of β-$NaLuF_4$ microcrystals.

associated with the transition from $^4S_{3/2}$, $^4F_{9/2}$, and $^4I_{9/2}$ levels to ground state of Er^{3+}, respectively. The intensities of emission bands were so strong that they can be clearly seen by the naked eyes even though they were under a low excitation power. The emission intensities are highly dependent on the Er^{3+} concentration. Initially, increasing Er^{3+} ion doping concentration, the intensity from all regions of the spectra increases rapidly and reaches a maximum. Then, a decrease appears at higher Er^{3+} concentrations due to the concentration quenching effect. As for the red emission, it is determined by the population of the $^4F_{9/2}$ level. The $^4F_{9/2}$ level is mainly populated by energy transfer between Er^{3+} ions when the doping concentration is increased, $^4I_{11/2}(Er^{3+})+{}^4I_{9/2}(Er^{3+}) \rightarrow {}^4I_{13/2}(Er^{3+})+{}^4F_{9/2}(Er^{3+})$ [26]. According to our experimental data, the optimum Er^{3+} concentration is 12 mol%Er^{3+} ions in S3 and 24 mol%Er^{3+} ions in S6. It is interesting to point out that the typical 541 nm green and 659 nm red emissions of Er^{3+} disappear in the spheres (S8; Figure 5(c)) and disks (S9; Figure 5(d)) and the intensities of emission bands of the two samples are poor. Comparing various morphologies, the emission intensity of hexagonal prism-like β-$NaLuF_4$: Er^{3+} microcrystals was found to be ~10^5 more efficient and brighter than others. The ranking of the emission intensities is UC-S3 > UC-S6 $\gg$ UC-S9 > UC-S8.

As for the different UC intensities of the four samples, there may be several factors playing a role. Since the shape and sizes of the microcrystals are different, it will bring a few uncertain factors that influence the UC behaviors through

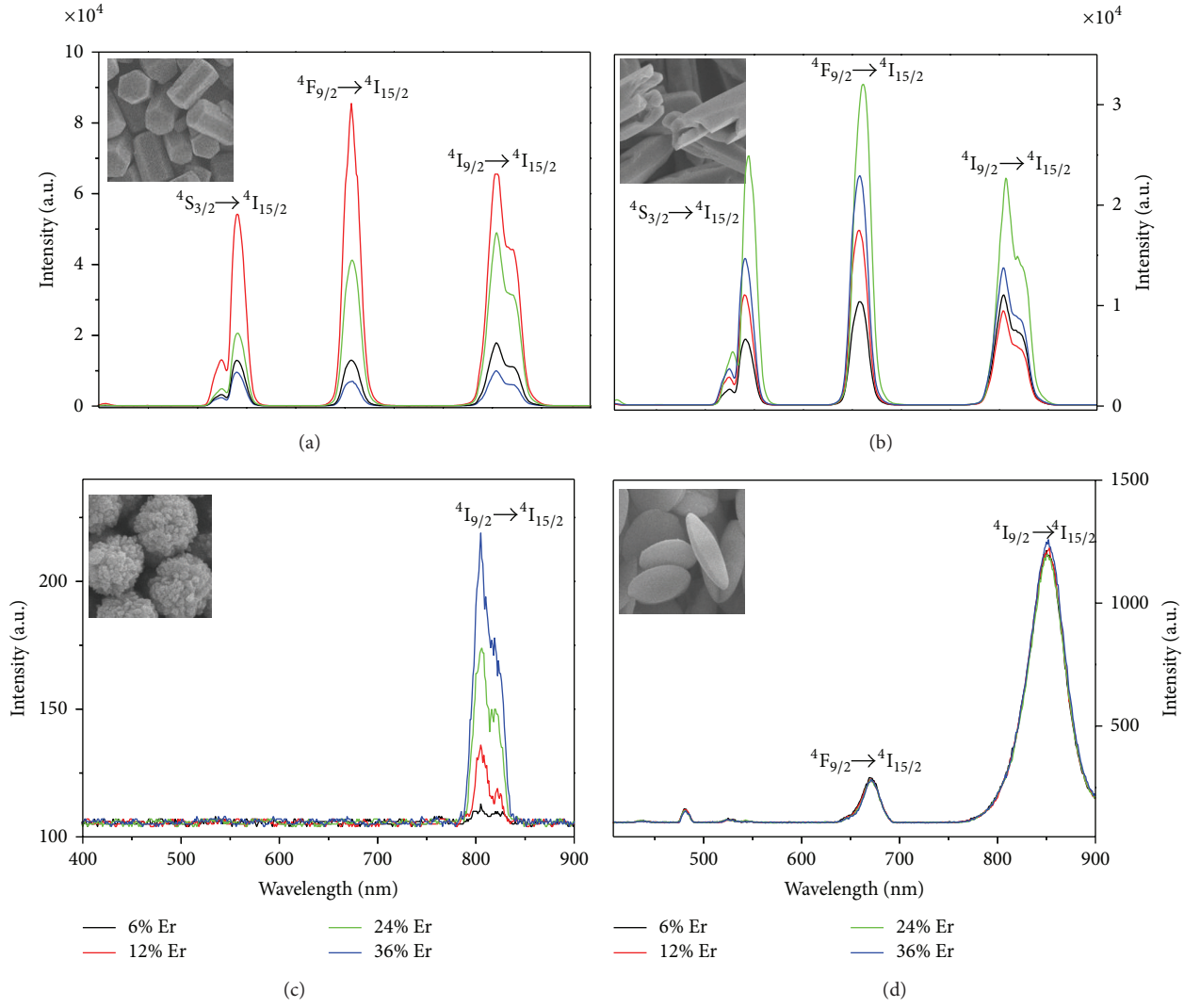

Figure 5: UCL spectra pumped by 1.54 μm laser diode with power density of 16 mW/mm^2 for β-$NaLuF_4$:x mol%Er^{3+} (x = 6, 12, 24, 36) synthesized using EDTA as the chelator for EDTA/Ln^{3+} ratio of 3 : 1 (a), using PVP as the chelator for PVP/Ln^{3+} ratio of 3 : 1 (b), and using Ct^{3-} as the chelator for Ct^{3-}/Ln^{3+} ratio of 2 : 1 (c) and 3 : 1 (d). Insets are corresponding high magnification SEM images of the samples. All of the samples were hydrothermally treated with the same condition except for the molar ratio of chelators/$Lncl_3$.

affecting the scattering and absorption of incident light, which decrease the defect concentrations [26, 29]. Moreover, the distinct difference of the emission intensities could be owing to the chelating and capping ability of surfactants. When an EDTA molecule chelates with one Ln^{3+} ion, all of its six binding sites participate in the reaction to develop a hexagonal structure. Furthermore, the chelate constant for EDTA (lgb = 18 ~ 19) is much larger than Ct^{3-} (lgb = 8 ~ 9) [7]. The structure stability coefficient of EDTA with Ln^{3+} ions is larger than Ct^{3-}, owing to its six binding sites (four binding sites in Ct^{3-}). The larger the stability coefficient is, the more closely the chelates combine with rare earth. Based on the above analysis, we can conclude that the difference in chelate structure results in the difference in morphology due to its influence on growth orientation, which can also be related to the difference in the emission intensity. Depending on the UC emission intensity, it is possible to vary particles size and shape and then to choose S3 for further characterization.

Figure 6 shows the UC emission spectra of hexagonal prisms (S3) $NaLuF_4$:12 mol% Er^{3+} under 1.54 μm laser diode at various pump powers. The 659 nm red emission is predominant, which is attributed to the $^4F_{9/2} \rightarrow {}^4I_{15/2}$ transitions of Er^{3+}. Besides, from the spectra, it is obvious that the emission intensities become stronger with increasing pump powers. It is well known that the relationship between the UC emission intensity I and the pump power P for unsaturated UC processes could be expressed as follows [30]:

$$I_{\text{em}} \propto P^n, \tag{1}$$

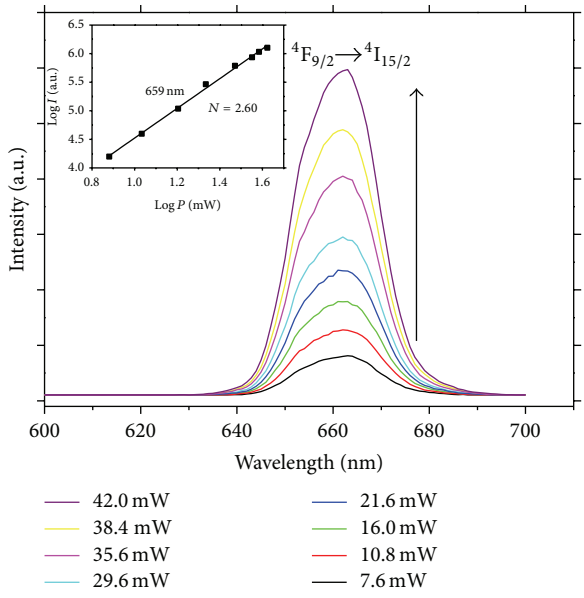

FIGURE 6: Power dependence of UC emission intensity of $^4F_{9/2} \rightarrow {}^4I_{15/2}$ emission of β-$NaLuF_4$:12 mol%Er^{3+} submicron crystals using EDTA as surfactant under 1.54 μm laser diode pump. Inset shows dependence of UC emission intensity on excitation powder.

where I_{em} is the fluorescent intensity, P is the pump power, and n is the absorbed photon numbers per visible photon emitted. For the strongest emission peak at 659 nm, a plot of log (I_{em}) versus log (P) yields a straight line with a slope n for the various power pumps as shown in the inset of Figure 6, and the n value obtained is equal to about 2.60. Hence, it is a three-photon process, which agrees with the three-step sequential transitions from the $^4I_{15/2}$ ground state to the $^4I_{13/2}$ intermediate state and then to the $^4F_{9/2}$ state of Er^{3+} in the excitation process.

3.4. Synergistic Effect of β-$NaLuF_4$:Er^{3+} Microcrystals. The excitation spectrum (Figure 7(a)) of β-$NaLuF_4$:12 mol%Er^{3+} (S3) with hexagonal prisms shape shows that if the 659 nm red emission is monitored, an excitation peak centered at 416 nm is observed corresponding to the $^4I_{15/2} \rightarrow {}^2H_{9/2}$ transition of Er^{3+} ion. Figure 7(b) presents the room temperature photoluminescence spectra under 416 nm single excitation, 1.54 μm single excitation, and 416 nm and 1.54 μm dual excitation. The emission band of Er^{3+} ions centered at 659 nm is observed under 416 nm and 1.54 μm single excitation, respectively. It is inconceivable that an observable enhancement of the red emission band appears under the dual excitation, which is stronger than the sum of red emission intensity under single excitation. To quantitatively describe the synergistic efficiency, the absolute enhancement rate (η) of red emission intensity can be defined as follows [20]:

$$\eta = \frac{I_3 - (I_1 + I_2)}{I_1 + I_2}, \quad (2)$$

where I_1, I_2, and I_3 are the integrated intensity of red emission bands under 416 nm excitation, under 1.54 μm excitation, and under 416 nm and 1.54 μm dual excitation, respectively, the excitation power of the 416 nm irradiation was fixed at 0.8 mW, and the excitation power (P) of 1.54 μm laser was adjusted from 2.2 mW to 42.0 mW. The results of absolute enhancement rate (η) of red emission (659 nm) for the as-prepared β-$NaLuF_4$:12 mol%Er^{3+} microcrystals with different shapes morphologies are shown in Figure 7(c). There is no synergistic effect on spheres and disks, because the intensities of emission bands are poor there is not exist the 659 nm emission The maximum absolute enhancement rate can be up to 8% in hexagonal prisms with the excitation powers $P_{416\,nm}$ = 0.8 mW and $P_{1.54\,\mu m}$ = 21.6 mW. It is clear that when $I_3 > (I_1 + I_2)$ it means that certain thermal energy dissipation should be eliminated and transferred to the excitation energy in the dual excitation process. As can be seen, the ranking of absolute enhancement rate values is η-S3 > η-S6. The red emission of $^4F_{9/2} \rightarrow {}^4I_{15/2}$ shows an unusual enhancement rate using different surfactants. We believe that the surfactants can influence the nonradiative process of these samples and cause these changes. Moreover, the different reflectance losses at the particle-air interface may influence the UC emissions of surface-modified $NaYF_4$:Yb, Er, which has been demonstrated in a recent report by Tan and coworkers [31].

3.5. Synergistic Mechanism Analyses. Considering the slope n and energy diagrams of Er^{3+}, the proposed pathways for the synergistic mechanism combined downconversion and upconversion under dual excitation are demonstrated in Figure 8. Under 416 nm excitation, which corresponds to the $^4I_{15/2} \rightarrow {}^2H_{9/2}$ transition of Er^{3+} ion, the 659 nm red emission band also represents the $^4F_{9/2} \rightarrow {}^4I_{15/2}$ transition of some Er^{3+} ions after successive multiphonon nonradiative relaxation from the $^2H_{9/2}$ to $^4F_{9/2}$ state. Under 1.54 μm excitation, Er^{3+} ions can absorb energy by ground state absorption (GSA) and excited state absorption (ESA) consecutively to populate their $^4I_{13/2}$ and $^4I_{9/2}$ states in succession. Then, some of Er^{3+} ions at $^4I_{9/2}$ level will nonradiatively relax (NR) to the $^4I_{11/2}$ level. $NaLuF_4$ host lattice owns lower phonon energy of less than 400 cm^{-1}, and the NR process (E_{gap} ~ 2500 cm^{-1}) can be realized according to energy gap law [32]. Then the crossrelaxation process from $^4I_{13/2}$ to $^4I_{11/2}$ and ESA process occur simultaneously: Er^{3+} ($^4I_{13/2} \rightarrow {}^4I_{15/2}$) and Er^{3+} ($^4I_{11/2} \rightarrow {}^4F_{9/2}$), which results in the 659 nm red upconversion emission ($^4F_{9/2} \rightarrow {}^4I_{15/2}$). Besides, the $^4I_{11/2}$ and $^4I_{13/2}$ levels are also populated through NR process in downconversion process. The energy in the $^4I_{11/2}$ and $^4I_{13/2}$ levels of Er^{3+} ions is usually dissipated via thermal energy; however, under the 416 nm and 1.54 μm coexcited, the Er^{3+} ions in the $^4I_{11/2}$ and $^4I_{13/2}$ levels from NR process can be

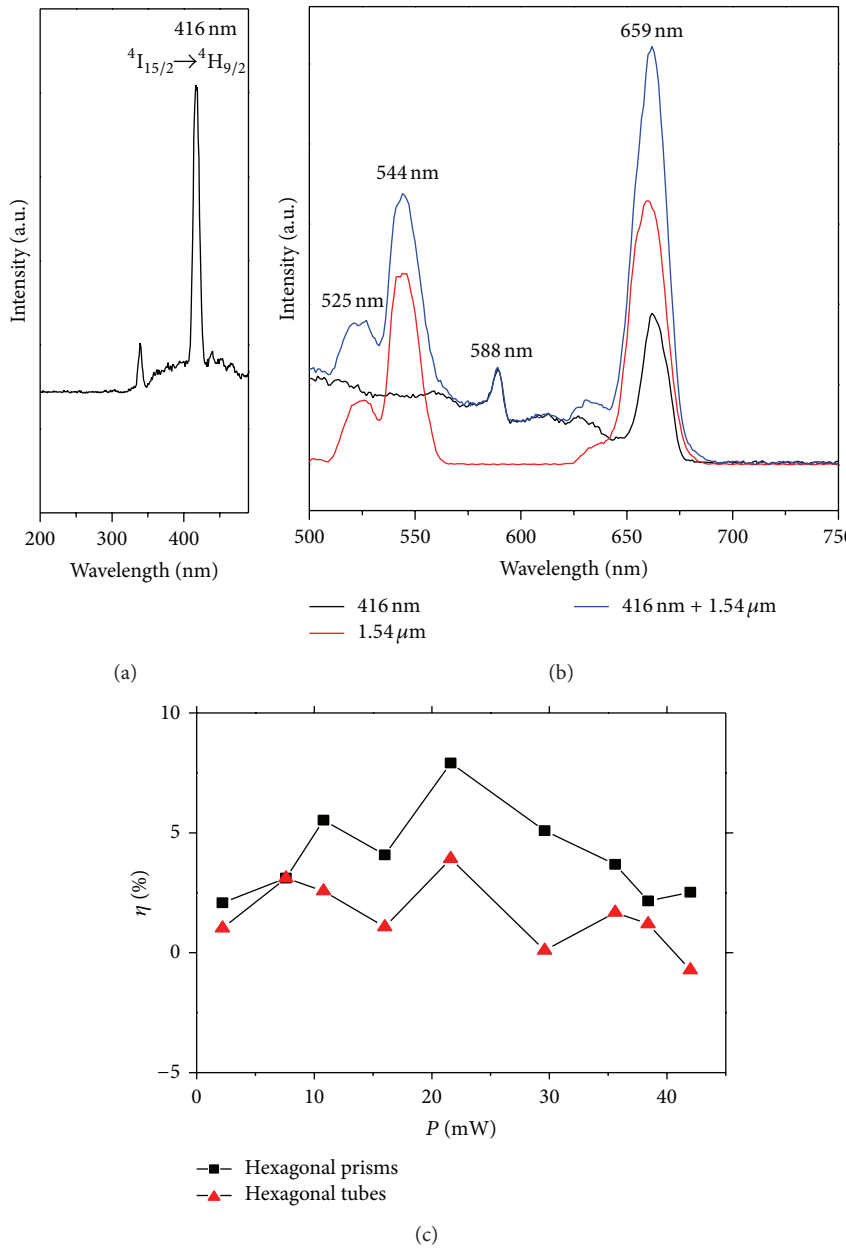

FIGURE 7: (a) Photoluminescence excitation spectra (λ_{em} = 659 nm) of β-$NaLuF_4$:12 mol%Er^{3+} with hexagonal prisms morphology; (b) visible photoluminescence spectra of β-$NaLuF_4$:12 mol%Er^{3+} under 416 nm excitation (black line), under 1.54 μm excitation (red line), and under 416 nm and 1.54 μm dual excitation (blue line) ($P_{416\,nm}$ = 0.8 mW, $P_{1.54\,\mu m}$ = 16 mW); (c) absolute enhancement (η) for the as-prepared β-$NaLuF_4$:12 mol%Er^{3+} crystals using different surfactants with increasing 1.54 μm laser power under 416 nm and 1.54 μm dual excitation.

excited again to the $^4F_{9/2}$ level by absorbing 1.54 μm photons. An energy loop chain can be described as follows:

$$^4I_{15/2} \longrightarrow {}^2H_{9/2} \longrightarrow {}^4I_{11/2} \longrightarrow {}^4F_{9/2} \longleftarrow {}^4I_{11/2} \longleftarrow {}^4I_{9/2} \longleftarrow {}^4I_{13/2} \longleftarrow {}^2H_{9/2} \longleftarrow {}^4I_{15/2}. \quad (3)$$

Therefore, the energy of nonradiative relaxation is excited again, enhancing the intensity of red emission ($^4F_{9/2} \rightarrow {}^4I_{11/2}$) under the dual excitation. As can be concluded, the Er^{3+} ions from the nonradiative relaxation process create a loop chain in the excitation circuit and offer a reexcited source.

4. Conclusions

In summary, we successfully synthesized β-$NaLuF_4$:Er^{3+} microcrystals with different surfactants by the hydrothermally method. The organic additives employed in the synthesis process played a significant role. It proved that the

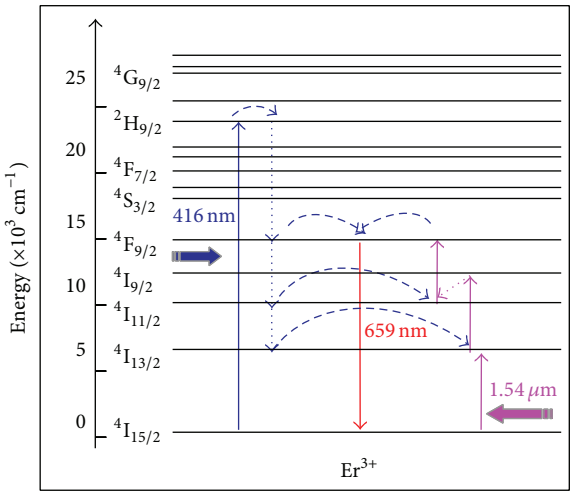

FIGURE 8: Synergistic effect of visible downconversion and IR upconversion in β-$NaLuF_4$:Er^{3+} phosphors photoexcited with both 416 nm and 1.54 μm photons.

chemical nature of the surfactants (EDTA, PVP-K30, and Ct^{3-}) differently acts with Ln^{3+} ions in solution, influencing the formation and growth process of the microcrystals. The EDTA-modified particles were found to be much more efficient and brighter than others, in which the intense 659 nm red emission band was observed. Under 416 nm and 1.54 μm dual excitation, the 8% absolute enhancement rate of the red emission band originating from the $^4I_{11/2}$ and $^4I_{13/2}$ states of Er^{3+} ion from the nonradiative relaxation process in the DC route can be excited again by absorbing the 1.54 μm IR photons in the UC route.

Conflict of Interests

The authors declare that there is no conflict of interests regarding the publication of this paper.

Acknowledgments

This work was supported by the key Project of National High Technology Research and Development Program of China (863 programs) (no. 2011AA050526), National Natural Science Foundation of China (no. 51032002), the Science and Technology Support Plan of Jiangsu Province (BE2011191), and the Funding of Jiangsu Innovation Program for Graduate Education (no. CXZZ12_0137) as well as the Fundamental Research Funds for the Central Universities.

References

[1] H.-X. Mai, Y.-W. Zhang, R. Si et al., "High-quality sodium rare-earth fluoride nanocrystals: controlled synthesis and optical properties," *Journal of the American Chemical Society*, vol. 128, no. 19, pp. 6426–6436, 2006.

[2] J.-C. Boyer, F. Vetrone, L. A. Cuccia, and J. A. Capobianco, "Synthesis of colloidal upconverting $NaYF_4$ nanocrystals doped with Er^{3+}, Yb^{3+} and Tm^{3+}, Yb^{3+} via thermal decomposition of lanthanide trifluoroacetate precursors," *Journal of the American Chemical Society*, vol. 128, no. 23, pp. 7444–7445, 2006.

[3] C. Li, Z. Quan, J. Yang, P. Yang, and J. Lin, "Highly uniform and monodisperse β-$NaYF_4$:Ln^{3+} (Ln = Eu, Tb, Yb/Er, and Yb/Tm) hexagonal microprism crystals: hydrothermal synthesis and luminescent properties," *Inorganic Chemistry*, vol. 46, no. 16, pp. 6329–6337, 2007.

[4] Y. Liu, D. Tu, H. Zhu, R. Li, W. Luo, and X. Chen, "A strategy to achieve efficient dual-mode luminescence of Eu^{3+} in lanthanides doped multifunctional $NaGdF_4$ nanocrystals," *Advanced Materials*, vol. 22, no. 30, pp. 3266–3271, 2010.

[5] M. Karbowiak, A. Mech, A. Bednarkiewicz, W. Stręk, and L. Kępiński, "Comparison of different $NaGdF_4$:Eu^{3+} synthesis routes and their influence on its structural and luminescent properties," *Journal of Physics and Chemistry of Solids*, vol. 66, no. 6, pp. 1008–1019, 2005.

[6] L. Wang, M. Lan, Z. Liu et al., "Enhanced deep-ultraviolet upconversion emission of Gd^{3+} sensitized by Yb^{3+} and Ho^{3+} in β-$NaLuF_4$ microcrystals under 980 nm excitation," *Journal of Materials Chemistry C*, vol. 1, no. 13, pp. 2485–2490, 2013.

[7] F. Wang and X. Liu, "Recent advances in the chemistry of lanthanide-doped upconversion nanocrystals," *Chemical Society Reviews*, vol. 38, no. 4, pp. 976–989, 2009.

[8] G. S. He, L.-S. Tan, Q. Zheng, and P. N. Prasad, "Multiphoton absorbing materials: molecular designs, characterizations, and applications," *Chemical Reviews*, vol. 108, no. 4, pp. 1245–1330, 2008.

[9] J. Zhou, Z. Liu, and F. Li, "Upconversion nanophosphors for small-animal imaging," *Chemical Society Reviews*, vol. 41, no. 3, pp. 1323–1349, 2012.

[10] D. K. Chatterjee, A. J. Rufaihah, and Y. Zhang, "Upconversion fluorescence imaging of cells and small animals using lanthanide doped nanocrystals," *Biomaterials*, vol. 29, no. 7, pp. 937–943, 2008.

[11] F. Shi, J. Wang, X. Zhai, D. Zhao, and W. Qin, "Facile synthesis of β-$NaLuF_4$:Yb/Tm hexagonal nanoplates with intense ultraviolet upconversion luminescence," *CrystEngComm*, vol. 13, no. 11, pp. 3782–3787, 2011.

[12] S. Zeng, J. Xiao, Q. Yang, and J. Hao, "Bi-functional $NaLuF_4$:Gd^{3+}/Yb^{3+}/Tm^{3+} nanocrystals: structure controlled synthesis, near-infrared upconversion emission and tunable magnetic properties," *Journal of Materials Chemistry*, vol. 22, no. 19, pp. 9870–9874, 2012.

[13] F. He, N. Niu, Z. Zhang et al., "Morphology-controllable synthesis and enhanced luminescence properties of β-$NaLuF_4$:Ln (Ln = Eu, Tb and Ce/Tb) microcrystals by solvothermal process," *RSC Advances*, vol. 2, no. 19, pp. 7569–7577, 2012.

[14] N. Niu, F. He, S. Huang, S. Gai, X. Zhang, and P. Yang, "Hierarchical bundles structure of β-$NaLuF_4$: facile synthesis, shape evolution, and luminescent properties," *RSC Advances*, vol. 2, no. 27, pp. 10337–10344, 2012.

[15] C. Li, Z. Quan, P. Yang, S. Huang, H. Lian, and J. Lin, "Shape-controllable synthesis and upconversion properties of lutetium fluoride (doped with Yb^{3+}/Er^{3+}) microcrystals by hydrothermal process," *Journal of Physical Chemistry C*, vol. 112, no. 35, pp. 13395–13404, 2008.

[16] Q. Liu, Y. Sun, T. Yang, W. Feng, C. Li, and F. Li, "Sub-10 nm hexagonal lanthanide-doped $NaLuF_4$ upconversion nanocrystals for sensitive bioimaging in vivo," *Journal of the American Chemical Society*, vol. 133, no. 43, pp. 17122–17125, 2011.

[17] S. Ivanova and F. Pellé, "Strong 1.53 μm to NIR-VIS-UV upconversion in Er-doped fluoride glass for high-efficiency

solar cells," *Journal of the Optical Society of America B: Optical Physics*, vol. 26, no. 10, pp. 1930–1938, 2009.

[18] T. Trupke, A. Shalav, B. S. Richards, P. Würfel, and M. A. Green, "Efficiency enhancement of solar cells by luminescent up-conversion of sunlight," *Solar Energy Materials and Solar Cells*, vol. 90, no. 18-19, pp. 3327–3338, 2006.

[19] S. Fischer, J. C. Goldschmidt, P. Löper et al., "Enhancement of silicon solar cell efficiency by upconversion: optical and electrical characterization," *Journal of Applied Physics*, vol. 108, no. 4, Article ID 044912, 2010.

[20] X. Wang and X. Yan, "Ultraviolet and infrared photon-excited synergistic effect in Er^{3+}-doped YbF_3 phosphors," *Optics Letters*, vol. 36, no. 22, pp. 4353–4355, 2011.

[21] K. Zheng, D. Zhao, D. Zhang, N. Liu, and W. Qin, "Ultraviolet upconversion fluorescence of Er^{3+} induced by 1560 nm laser excitation," *Optics Letters*, vol. 35, no. 14, pp. 2442–2444, 2010.

[22] S. Zheng, Y. Zhou, D. Yin, X. Xu, Y. Qi, and S. Peng, "Improvement of 1.53 μm band fluorescence and energy transfer in Er^{3+}/Ce^{3+} codoped tellurite glasses," *Journal of Alloys and Compounds*, vol. 566, pp. 90–97, 2013.

[23] K. Maheshvaran, S. Arunkumar, V. Sudarsan, V. Natarajan, and K. Marimuthu, "Structural and luminescence studies on Er^{3+}/Yb^{3+} co-doped boro-tellurite glasses," *Journal of Alloys and Compounds*, vol. 561, pp. 142–150, 2013.

[24] R. Dahal, C. Ugolini, J. Y. Lin, H. X. Jiang, and J. M. Zavada, "Current-injected 1.54 μm light emitting diodes based on erbium-doped GaN," *Applied Physics Letters*, vol. 93, no. 3, Article ID 033502, 2008.

[25] G. D. Webler, M. J. M. Zapata, G. S. Maciel et al., "Influence of impurities on the luminescence of Er^{3+} doped $BaTiO^3$ nanophosphors," *Journal of Nanomaterials*, vol. 2014, Article ID 708719, 9 pages, 2014.

[26] S. Shionoya, W. M. Yen, and T. Hase, *Phosphor Handbook*, CRC Press, New York, NY, USA, 2007.

[27] Z. Q. Li and Y. Zhang, "Monodisperse silica-coated Polyvinylpyrrolidone/$NaYF_4$ nanocrystals with multicolor upconversion fluorescence emission," *Angewandte Chemie*, vol. 118, no. 46, pp. 7896–7899, 2006.

[28] L. S. Cavalcante, J. C. Sczancoski, M. Siu Li, E. Longo, and J. A. Varela, "β-$ZnMoO_4$ microcrystals synthesized by the surfactant-assisted hydrothermal method: growth process and photoluminescence properties," *Colloids and Surfaces A: Physicochemical and Engineering Aspects*, vol. 396, pp. 346–351, 2012.

[29] C. Huang, *Coordination Chemistry of Rare Earth Elements*, Science Publishing Press, Beijing, China, 1997.

[30] M. Pollnau, D. R. Gamelin, S. R. Lüthi, H. U. Güdel, and M. P. Hehlen, "Power dependence of upconversion luminescence in lanthanide and transition-metal-ion systems," *Physical Review B—Condensed Matter and Materials Physics*, vol. 61, no. 5, pp. 3337–3346, 2000.

[31] M. C. Tan, L. Al-Baroudi, and R. E. Riman, "Surfactant effects on efficiency enhancement of infrared-to-visible upconversion emissions of $NaYF_4$:Yb-Er," *ACS Applied Materials and Interfaces*, vol. 3, no. 10, pp. 3910–3915, 2011.

[32] J. M. F. Van Dijk and M. F. H. Schuurmans, "On the nonradiative and radiative decay rates and a modified exponential energy gap law for 4f-4f transitions in rare-earth ions," *The Journal of Chemical Physics*, vol. 78, no. 9, pp. 5317–5323, 1983.